

Confinement of pure electron plasmas in the Columbia Non-neutral Torus

John W. Berkery,^{a)} Thomas Sunn Pedersen, Jason P. Kremer, Quinn R. Marksteiner, Remi G. Lefrancois, Michael S. Hahn, and Paul W. Brenner

Department of Applied Physics and Applied Mathematics, Columbia University, New York, New York 10027

(Received 29 March 2007; accepted 8 May 2007; published online 19 June 2007)

The Columbia Non-neutral Torus (CNT) [T. S. Pedersen, J. P. Kremer, R. G. Lefrancois, Q. Marksteiner, N. Pomphrey, W. Reiersen, F. Dahlgreen, and X. Sarasola, *Fusion Sci. Technol.* **50**, 372 (2006)] is a stellarator used to study non-neutral plasmas confined on magnetic surfaces. A detailed experimental study of confinement of pure electron plasmas in CNT is described here. Electrons are introduced into the magnetic surfaces by placing a biased thermionic emitter on the magnetic axis. As reported previously, the insulated rods holding this and other emitter filaments contribute to the radial transport by charging up negatively and creating $E \times B$ convective transport cells. A model for the rod-driven transport is presented and compared to the measured transport rates under a number of different conditions, finding good agreement. Neutrals also drive transport, and by varying the neutral pressure in the experiment, the effects of rod-driven and neutral-driven transport are separated. The neutral-driven electron loss rate scales linearly with neutral pressure. The neutral driven transport, presumably caused by electron-neutral collisions, is much greater than theoretical estimates for neoclassical diffusion in a classical stellarator with strong radial electric fields. In fact the confinement time is on the order of the electron-neutral collision time. Ion accumulation, electron attachment, and other effects are considered, but do not explain the observed transport rates. © 2007 American Institute of Physics. [DOI: 10.1063/1.2745814]

I. INTRODUCTION

A great amount of attention has been paid to the stellarator optimization,^{1,2} that is, the reduction of ripples in the magnetic field³ and creation of quasisymmetry⁴ to enhance confinement time. The importance of the radial electric field on confinement in stellarators has also been recognized.^{1,5,6} The extreme electric field (where “extreme” refers to $e\Delta\phi/T_e \gg 1$) of a non-neutral plasma should lead to excellent confinement of such a plasma in a stellarator, even a classical stellarator, $\tau \propto \tau_c(a/\lambda_D)^4$, with τ_c being the collision time.⁷

The Columbia Non-neutral Torus (CNT) (Ref. 8) studies pure electron plasmas confined on magnetic surfaces. This work is similar to the so-called “stellarator diode” work^{9–13} which was concerned with mapping magnetic surfaces by contours of constant emission from an electron emitter in a stellarator. CNT is concentrated on understanding the equilibrium, stability, and transport of the pure electron plasmas created by this thermionic emission. In this paper, we focus on the question of pure electron plasma transport in CNT. As shown recently,¹⁴ the pure electron plasmas in CNT satisfy the plasma criterion $a/\lambda_D \approx 10 \gg 1$ as well as the criterion for having an extreme electric field $e\Delta\phi/T_e \approx 20 \gg 1$. Quasineutral plasmas generally have $a/\lambda_D \gg 1$ and $e\Delta\phi/T_e$ of order unity whether the electric potential is created by plasma transport (ambipolar electric fields) or imposed by the experimentalist through the use of biased limiters,¹⁵ biased probes,¹⁶ or electron emitting cathodes.¹⁷

The results presented in this article focus primarily on a parameter regime where the neutral pressure, $p_n < 1.5 \times 10^{-7}$ Torr, plasma potential, $|\phi_p| < 400$ V, and magnetic

field strength, $B > 0.01$ T. For these parameters, the plasmas are stable and do not exhibit sudden confinement jumps. However, outside this parameter range, different physics appears. At very high bias voltages and very low magnetic fields, the emission current has discontinuous jumps. At very high neutral pressures, ion driven instabilities appear. The plasma behavior in these parameter regimes will be discussed in detail in future publications.

Two distinct transport mechanisms for pure electron plasmas have been identified in CNT, one related to the perturbing presence of internal rods, and another related to background neutrals. In Sec. III the rod-driven transport is discussed, including the dependence of emission current on magnetic field and emitter bias in this regime. In Sec. IV, the electron loss rate is separated into rod-driven and neutral-driven parts and the dependence of each on the magnetic field is examined. Section V discusses the confinement time in CNT and makes comparisons to other relevant time scales. In Sec. VI possible causes for the enhanced level of neutral driven transport seen in these plasmas are presented. Since the purpose of this work is to investigate the transport mechanisms and their dependencies on various plasma parameters, the confinement times here are in general lower than the best confinement time achieved in CNT, 20 ms, reported previously.¹⁴

II. EXPERIMENTAL SETUP

Pure electron plasmas are created in steady state in CNT by a heated, biased electron emitter placed on the magnetic axis (see Fig. 1). Parallel transport fills the magnetic axis field line with electrons, and then cross-surface transport fills the confining volume of magnetic surfaces. The emitter is

^{a)}Electronic mail: jwb2112@columbia.edu

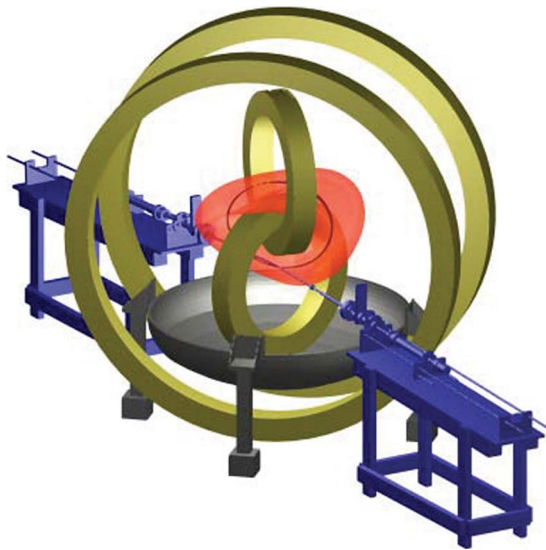


FIG. 1. (Color online) A cutaway drawing of the CNT device, showing the magnetic field coils, the confining volume, the magnetic axis, and the two filament rods. The electron emitter rod is positioned such that the emitter is placed on the magnetic axis.

located physically inside the plasma, and the plasma reaches an equilibrium density; a steady-state is reached between electron emission and loss. The confinement time of electrons is simply the total number of electrons divided by the electron loss rate, $\tau = eN_e/I_e$. The electron loss rate (in C/s or A) is equal to the emission current, which is easily measured. The total number of electrons N_e can be estimated from an equilibrium reconstruction from experimentally measured radial profiles of temperature and either density or potential.¹⁴ In this paper we explore the dependence of the electron loss rate and confinement time on the magnetic field, emitter bias, and neutral pressure, and discuss the dominant transport mechanisms.

III. ROD-DRIVEN TRANSPORT

In the rod-driven transport regime, the dominant mechanism of electron loss is the electrostatic perturbation caused by the negatively charged insulating rods.¹⁴ Convective $E \times B$ cells are set up from the static confining magnetic field and the electric field from the negatively charged rods. The drift is into the plasma on one side of the rod and out of the plasma on the other. Due to a density gradient there is a net loss of particles from the confining region. A schematic of this mechanism appears in Fig. 2.

In order to calculate the transport of electrons due to the rods, it is necessary to calculate their density and velocity as functions of r and θ near the rod. Electrons in a Boltzmann density distribution are represented by $n_e = n_\infty \exp(e\phi/T_e)$, and we assume that the potential is given by $\phi = \phi_0 \exp((r_0 - r)/\lambda_D)$, where r_0 is the rod radius. This estimate for the potential is the standard textbook Debye-screened potential, which is arrived upon by solving Poisson's equation for a linearized Boltzmann density distribution, $\exp(e\delta\phi/T_e) \approx 1 + e\delta\phi/T_e$. Our model does not accurately take into account that this linearization is inaccurate near the rod, since

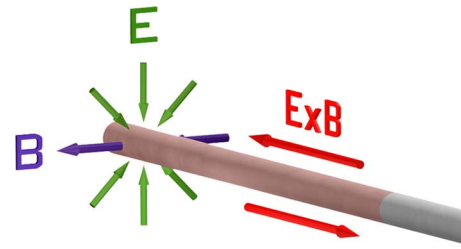


FIG. 2. (Color online) A schematic of the convective particle transport caused by the presence of the insulating rods. The magnetic field indicated is the static confining field and the electric field is the field from the charged up rods.

$|-e\delta\phi/T_e|$ is not small near the rod and $n_e \approx 0$ there, i.e., there is no space charge there to do the regular Debye shielding. Here $\delta\phi$ is the difference between the equilibrium plasma potential and the potential in the presence of the negatively charged rod. Further work is continuing on a numerical calculation of the rod-driven transport, but in order to provide an analytically tractable estimate, we will proceed with the above estimate for the potential profile.

If \mathbf{B} is in the $-\hat{x}$ direction, \mathbf{E} is directed radially inward, and \hat{z} is outward along the rod (Fig. 2), then

$$\mathbf{v} = \frac{\mathbf{E} \times \mathbf{B}}{B^2} = -\frac{d\phi \sin \theta}{dr} \frac{\hat{z}}{B}. \quad (1)$$

Using experimentally measured values of $n_\infty \approx 7.5 \times 10^{11} \text{ m}^{-3}$, $r_0 = 6.35 \times 10^{-2} \text{ m}$, and $T_e = 4 \text{ eV}$,¹⁴ we can calculate the flux of electrons ($n_e v$) near the rod. This is shown as a contour plot in Fig. 3. The transport is very low very close to the rod (due to the very low electron density), peaks a couple of Debye lengths away from the rod, and falls off exponentially far away from the rod because of the Debye screening of the electric field.

The current of electrons transported out in this manner is

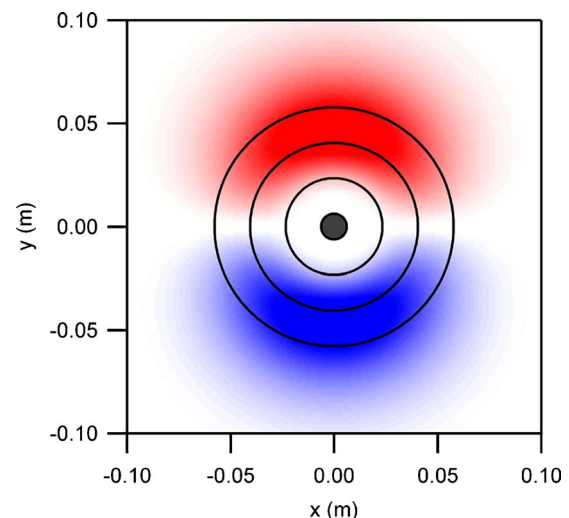


FIG. 3. (Color online) Contour plot of $n_e v$ [$\text{m}^{-2}\text{s}^{-1}$] near an insulated rod. The red region above the rod indicates inward flux, while the blue region below the rod indicates outward flux. The black circles represent distances of λ_D , $2\lambda_D$, and $3\lambda_D$ away from the rod.

$$I_e = N_r e \int_{\pi}^{2\pi} \int_{r_0}^{\infty} (n_e v) r dr d\theta, \quad (2)$$

where N_r is the number of rods, e is the electron charge, and $n_e v$ is the flux of electrons, which is integrated over the bottom half of the rod. Using the above expressions for n_e and ϕ , and with $\phi_0 = -C_0 T_e / e$, Eq. (2) reduces to

$$I_e = (2N_r)(\epsilon_0 n_e)^{1/2} (T_e)^{3/2} (eB)^{-1} \mathcal{F}, \quad (3)$$

where \mathcal{F} is a dimensionless integral given by

$$\mathcal{F} = \int_{r_0}^{\infty} C_0 \lambda_D^{-2} \exp\left[\frac{r_0 - r}{\lambda_D}\right] - C_0 \exp\left[\frac{r_0 - r}{\lambda_D}\right] r dr. \quad (4)$$

The above integral is analytically solvable and yields the following expression that depends only on the values of r_0/λ_D and C_0 ,

$$\mathcal{F} = \frac{r_0}{\lambda_D} (1 - e^{-C_0}) + \ln(C_0) - \text{Ei}(-C_0) + \gamma, \quad (5)$$

where Ei is the exponential integral and $\gamma = 0.5772$ is the Euler-Mascheroni constant.

For a quasineutral plasma $C_0 = 1/2(\ln(m_i/2\pi m_e) + 1)$, which, with N_2^+ as the dominant ion, is equal to 5. The true value of C_0 in the pure electron plasma, and hence the floating potential of the insulated rod, is not known with certainty. Because the ion fraction is very small, the rods will charge up to a significantly more negative potential than in a quasineutral plasma. An estimate can be obtained by adding the term $-\ln(f_i)$ to C_0 , which is a first-order correction for plasmas with an ion fraction $f_i = n_i/n_e$. For the conditions considered here, the ion fraction in CNT is $f_i \approx 0.005$, which gives a value of $C_0 \approx 10$.

For the value of $r_0/\lambda_D = 0.37$ from the present parameters, \mathcal{F} increases from 2.55 to 3.94 in the range of C_0 from 5 to 20. In the calculation for Fig. 3, $C_0 = 10$ was used. A higher C_0 causes the region of transport to widen and move farther out radially, and causes the total integrated transport given by Eq. (3) to increase. The assumption that the potential drops off exponentially with the bulk plasma Debye length as the relevant length scale makes the radius of peak transport, and \mathcal{F} , rather insensitive to C_0 . A full nonlinear self-consistent calculation of the screening would show a very low density ‘‘hollow’’ shell around the rod, with the potential falling off rather slowly, and a peak transport region located farther from the rod than what is calculated here. The electrostatic perturbation due to the rod and its associated radial transport is therefore larger than what is calculated here. In addition to the simplified sheath potential profile and the uncertainty in C_0 , there are a few other simplifications in the above model. It ignores the variation in magnetic field, plasma density, and temperature along the rod. Also, it ignores the inward transport on the top side of the rod. This is equivalent to assuming a density that is constant inside the magnetic surfaces and is zero outside. In other words, electrons transported out are lost to the open field lines at the edge, while no electrons are transported from outside the closed flux surfaces to the inside. Despite all of these simplifications, we will see in Secs. III B and IV B that this

simple model of rod-driven transport captures the trend of the data well, and is in rough quantitative agreement with the observed transport rates.

A. Effect of magnetic field

In the rod-driven transport regime, the magnetic field is expected to have a B^{-1} scaling effect on the electron loss rate. To test this, the emission current was measured as a function of magnetic field strength (on axis) at a neutral pressure of $p_n \approx 7 \times 10^{-9}$ Torr, and an emitter bias of -400 V. These measurements were presented in Ref. 14 and showed the expected B^{-1} scaling. We have observed that for a fixed emitter bias, the electron density and temperature are essentially independent of the magnetic field strength. If this were not the case, then a simple B^{-1} dependence would not be expected from Eq. (3), since the transport rate depends on density and temperature, as well as on the strength of the B -field.

Similar scaling, and very similar magnitude, of emission current vs magnetic field was seen in stellarator diode studies in the Auburn torsatron,⁹ where an insulated rod was also used. They reported a scaling of $B^{-0.87}$, but B^{-1} is within the error bars of their measurements. Similar studies in the Uragan-3M torsatron showed $B^{-0.84}$ and $B^{-0.67}$ scaling.¹⁰

B. Effect of emitter bias

By changing the emitter bias while at a constant magnetic field, the temperature and density of the electron plasma are changed. From -100 to -400 V, the electron temperature increases approximately linearly from 1.5 eV to 5.8 eV.¹⁸ The density has been measured at $p_n = 2 \times 10^{-8}$ Torr, $B = 0.02$ T, and -200 V bias to be $n_e \approx 7.5 \times 10^{11} \text{ m}^{-3}$.¹⁴ The density should vary linearly with emitter bias since the emitter bias sets the plasma potential and the plasma potential is linearly related to the charge density, and therefore the electron density, through Poisson’s equation. Although accurate measurements of n_e in CNT are difficult,¹⁹ there is some indication that this is the case.¹⁸ For potentials less negative than -100 V, measurements have been difficult due the very low electron density, but the density continues to decrease as the bias potential approaches zero whereas the electron temperature appears to rise.

For these experiments, the emission current (i.e., the electron loss rate) was measured as a function of emitter bias (i.e., plasma potential). We compare this measured electron loss rate to the expected loss rate as calculated from Eq. (3).

Figure 4 shows this comparison. In this case the markers are the measured electron loss rate (emission current) as the emitter bias was increased. This is analogous to the current-voltage characteristic of a stellarator diode.^{10,11} The solid line represents the modeled values calculated from Eq. (3) using the measured n_e and T_e , and with $C_0 = 10$. The trend of the data is captured well by the model, but the magnitude is underestimated somewhat. As mentioned previously, our model is expected to underestimate the rod driven transport.

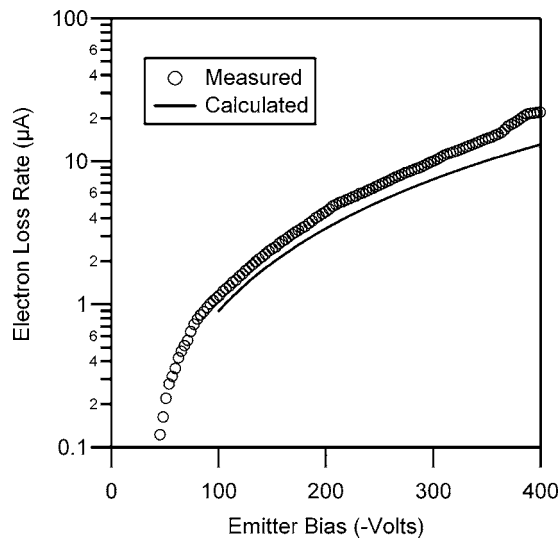


FIG. 4. Electron loss rate vs emitter bias for increasing negative potential with $B=0.02$ T and $p_n=2 \times 10^{-8}$ Torr. The measured current is represented by the points and the line is calculated according to the model of rod-driven transport through Eq. (3).

IV. NEUTRAL-DRIVEN TRANSPORT

A. Effect of neutral pressure

When the neutral pressure is increased, loss of electrons due to collisions with neutrals becomes noticeable and eventually dominant over rod-driven transport. By varying the neutral pressure, the two transport processes can be separated. Figure 5 shows the emission current from two sets of experiments in which the magnetic field was held constant while the neutral pressure was increased. The electron loss rate is seen to follow a linear trend, $I_e = I_r + I_n$, where the constant I_r , the loss at zero neutral pressure, is the transport unrelated to neutrals, and $I_n \propto p_n$ is the transport due to the neutrals. Since it has been found that the transport at low

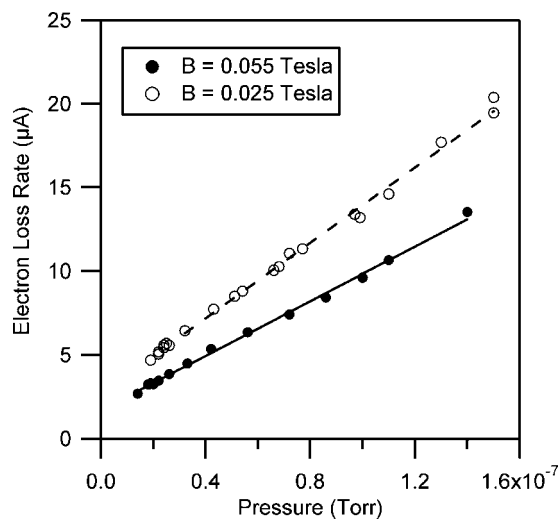


FIG. 5. Electron loss rate vs neutral pressure for two representative magnetic field values in the low pressure regime ($\leq 1.5 \times 10^{-7}$ Torr).

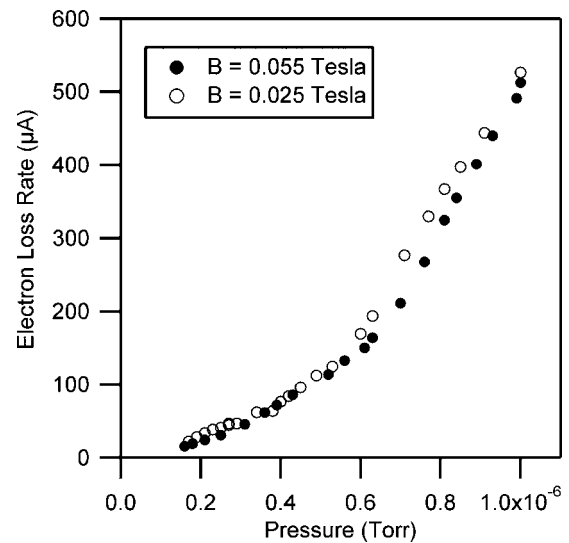


FIG. 6. Electron loss rate vs neutral pressure for two representative magnetic field values in the high pressure regime (1.5×10^{-7} Torr $< p_n < 1 \times 10^{-6}$ Torr). These data are a continuation of the data in Fig. 5.

neutral pressures is strongly dominated by the rods,¹⁴ we identify I_r as the rod driven transport even though there may be other transport processes included in I_r .

One can now easily separate the two transport processes, and compare their magnitudes. For example, for the case of $B=0.02$ T, at low pressure, $p_n=7 \times 10^{-9}$ Torr, the ratio of I_n/I_r is about 0.3, i.e., the rod driven transport dominates by a factor of 3.3, while at high neutral pressure, $p_n=1 \times 10^{-7}$ Torr, $I_n/I_r \approx 4.5$, i.e., the neutral driven transport dominates by a factor of 4.5. The data discussed in Sec. III A is clearly in the rod-driven transport regime because of the low neutral pressure (7×10^{-9} Torr). The data presented in Sec. III B (and Fig. 4) was taken at $p_n=2 \times 10^{-8}$ Torr, in a neutral pressure range where the neutral-driven transport is becoming important.

For the neutral pressure range covered in Fig. 5, I_n scales linearly with pressure, so the transport is proportional to the electron-neutral collision frequency. The linear dependence of emission current on neutral pressure has also been seen before in electron confinement experiments,^{9,20,21} all at higher neutral pressures than what is measured here. As discussed later, this linear relationship is expected from neoclassical transport theory.

When the neutral pressure in CNT is increased above about 1.5×10^{-7} Torr, I_n begins to deviate from the simple linear proportionality to neutral pressure—it grows faster than linearly (see Fig. 6). In this range the emission current scales like p^α with α between 2.3 and 2.5 for all magnetic field values above $B=0.02$ T. The transition from linear to nonlinear dependence of transport on neutral pressure is likely caused by the onset of ion-related instabilities, which begin to appear in this elevated neutral pressure range. These instabilities will be described in a future publication.

B. Effect of magnetic field

Using the above mentioned technique of varying the neutral pressure in the range 7×10^{-9} – 1.5×10^{-7} Torr, I_n

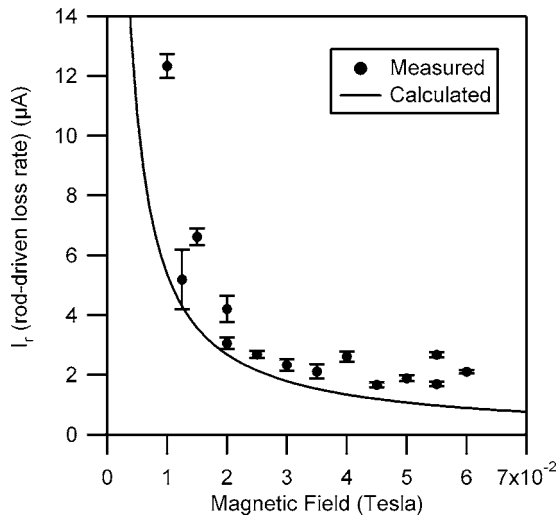


FIG. 7. The electron loss rate due to the rods (I_r) for different magnetic field values. The markers are the measured values and the line is calculated from Eq. (3).

and I_r were measured for different magnetic field values, while holding the emitter bias constant at -200 V. Figure 7 shows the values of I_r , the intercepts of the linear measurements. As already discussed, we interpret I_r as the rod-driven transport. Also shown in the figure is the modeled rod-driven electron loss rate, from Eq. (3), with $C_0=10$, $N_r=2$, and using $n_e=7.5 \times 10^{11} \text{ m}^{-3}$, and $T_e=4$ eV. These are the measured values at a bias of -200 V, a neutral pressure of 2×10^{-8} Torr, and magnetic field of 0.02 V. In these calculations it is assumed that the changing magnetic field and neutral pressure do not change the electron temperature and density. This is consistent with experimental findings.

The model of the rod-driven transport, which is proportional to B^{-1} , captures the trend of I_r well, while again underestimating the magnitude, presumably because of the aforementioned simplifications made in the model.

As defined, I_n is the part of the electron loss rate that scales linearly with neutral pressure so it is caused by the presence of neutrals. Figure 8 shows the neutral-driven electron loss rate divided by the neutral pressure as a function of the magnetic field. These data are obtained from the slopes of the emission current vs neutral pressure measurements, such as the examples in Fig. 5. Clearly the neutral-driven transport is not proportional to B^{-1} , as was the case with the rod-driven transport.

A curve fit is also shown on the plot, with the form $I_n/p_n=53.3+0.244 \times B^{-1.5}$ A/Torr. One could choose other functional forms for the curve fit but this one fits the data very well. We interpret this result as implying that there are two transport processes associated with the neutrals, one that scales with $B^{-1.5}$, and another which is independent of the magnetic field strength. Candidates for each of these will be discussed in the following sections.

V. CONFINEMENT TIME

The measured confinement time due to neutral-driven transport is given by $\tau=eN_e/I_n$. From measured profiles of

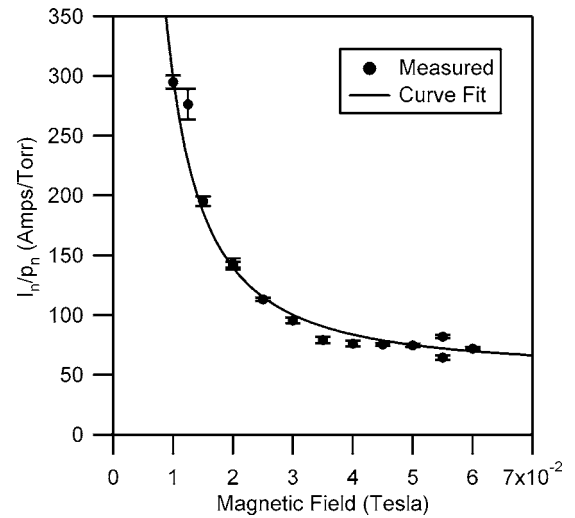


FIG. 8. The slopes ($C_0=I_n/p_n$) of the emission current vs neutral pressure data for different magnetic field values (for example, see Fig. 5). The markers are measured values and the line is a curve fit.

the density, temperature, and potential, equilibrium reconstructions can be carried out which show that at a bias voltage of -200 V, $N_e \approx 10^{11}$.¹⁴ For this bias voltage, and at $p_n=2 \times 10^{-8}$ Torr, and $B=0.06$ T, using $I_n/p_n \approx 62$ A/Torr from Fig. 8, the neutral-driven confinement time is $\tau \approx 1.3 \times 10^{-2}$ s. Because of rod-driven transport, the true measured confinement time is less than this.

It is well-known that for a quasineutral plasma in a classical stellarator transport due to direct orbit losses can be very large, even dwarfing anomalous transport. CNT is a classical stellarator with large helical ripple, and in the absence of a strong electric field, the neoclassical confinement time would be expected to be on the order of

$$\tau_d \approx \frac{a}{\mathbf{v}_{\nabla B+R}} \approx ea^2B/T_e, \quad (6)$$

where

$$\mathbf{v}_{\nabla B+R} = - \left(\frac{1}{2}mv_{\perp}^2 + mv_{\parallel}^2 \right) \frac{\nabla B \times \mathbf{B}}{eB^3} \quad (7)$$

is the particle drift velocity due to ∇B and magnetic curvature. For the experimental conditions discussed here, we estimate $\tau_d \approx 3.4 \times 10^{-4}$ s, which is much less than the measured confinement time. Therefore, the vast majority of electrons must be on confined orbits. This is actually expected because of the strong electric field in CNT. In the presence of a strong electric field, one expects a vastly improved confinement time, because the ripple trapped particles are forced to circulate poloidally because of the $E \times B$ drift associated with the strong radial electric field. In this case, the collisionless particles remain close to the magnetic surfaces, and cross-surface particle transport will be proportional to the collision frequency. In our case, the electron-neutral collision frequency ν_{en} is an order of magnitude larger than ν_{ee} , so the dominant collisional process for the electrons is electron-neutral collisions, not electron-

electron collisions. The resulting particle diffusion coefficient is²²

$$D_\nu = \nu_{en} \left(\frac{\mathbf{v}_{\nabla B+R}}{\omega_E} \right)^2 \times \left(\frac{\epsilon^2}{\epsilon_r^2} \frac{1}{\sqrt{\epsilon + 2\epsilon_h - \sqrt{2\epsilon_h}}} \right), \quad (8)$$

where ω_E is the $E \times B$ frequency. For an optimized stellarator, the second bracketed term involving ϵ (the poloidal ripple), ϵ_r (the inverse aspect ratio r/R), and ϵ_h (the helical ripple), can be made small, but for a classical stellarator such as CNT, it is of order unity, possibly larger. Setting this term to 1, estimating the diffusion-limited confinement time as $\tau_e \approx a^2/D_\nu$, and noting that $E \approx \Delta\phi/a$, and $e\Delta\phi/T_e \approx a^2/\lambda_D^2$ in a pure electron plasma with minor radius a , the confinement time in CNT can be crudely approximated as⁷

$$\tau_e \approx \tau_{en} a^4 / \lambda_D^4. \quad (9)$$

In CNT, which has $a/\lambda_D \approx 10$, one should therefore expect that the neutral-driven transport would lead to a confinement time on the order of 10^4 electron-neutral collision times. The significant neoclassical transport reduction caused by the strong electric field has been confirmed, for quasineutral plasmas with modest electric fields, by direct numerical particle orbit calculations.²² Equation (8) and consequently Eq. (9) are valid when $\nu_{en} \ll \omega_E$. In CNT, $\omega_E \approx 5.5 \times 10^4 \text{ s}^{-1}$, much larger than ν_{en} even at the higher end of neutral pressures discussed here, so Eq. (9) should apply to the plasmas being studied here. We note that our experimental finding that the neutral-related confinement time is proportional to the electron-neutral collision time is consistent with the scaling in Eq. (9), but as we will show in the following, the magnitude of the measured confinement time is inconsistent with Eq. (9).

First, the crude approximation $E \approx (T_e/e)(a/\lambda_D^2)$ is correct for scaling purposes, but significantly off in magnitude. Since E has been measured in CNT, it can be used to calculate ω_E and therefore τ_e directly. A potential drop of $\sim 75 \text{ V}$ over $\sim 15 \text{ cm}$ gives an electric field of approximately 500 V/m , which was used to find the value of ω_E above. From Eq. (8) we find

$$\tau_e = \tau_{en} (\tau_d \omega_E)^2, \quad (10)$$

and with the calculated values of τ_d and ω_E , the confinement time should be $\tau_e = 350 \tau_{en}$. This is much less than 10^4 times, because the simplicity of the scaling approximation for E does not take into account the complex geometry of the CNT plasma. Nonetheless, the neoclassical prediction is that the confinement time should be many orders of magnitude greater than the collision time. We will now show that this is not seen experimentally.

The electron-neutral collision time, $\tau_{en} = 1/\nu_{en}$, is calculated by the following equation:

$$\nu_{en} = n_n \left(\frac{2}{m_e} \right)^{1/2} \int_0^\infty \left(\frac{2\mathcal{E}}{\pi^{1/2} (T_e)^{3/2}} \right) Q_{en} e^{-\mathcal{E}/T_e} d\mathcal{E}, \quad (11)$$

where Q_{en} is the electron-neutral elastic scattering collision cross section and is a function of the neutral species and the electron energy (\mathcal{E}). For these experiments, molecular nitrogen is the most abundant neutral species, so at $T_e = 4 \text{ eV}$ and

$p_n = 2 \times 10^{-8} \text{ Torr}$, we find, using published cross-sectional data,²³ that $\nu_{en} \approx 100 \text{ s}^{-1}$ i.e., $\tau_{en} \approx 1 \times 10^{-2} \text{ s}$.

We see that the measured neutral-driven confinement time, $\tau \approx 1.3 \times 10^{-2} \text{ s}$, is approximately equal to the electron-neutral collision time scale and is orders of magnitude below the theoretical neoclassical confinement time ($350 \tau_{en}$). This close match between measured τ and calculated τ_{en} is partially an artifact of the conditions we have chosen for the calculations. Figure 8 shows that the measured neutral-driven confinement time is dependent on p_n and B , while the calculation of τ_{en} is dependent only on p_n . For a lower B field, the electron-neutral collision time is the same, but the measured confinement time is less, implying that on average less than one electron-neutral collision is sufficient for an electron to be lost. In reality, uncertainties in the absolute neutral pressure measurement and collision cross section prevent us from making an exact statement about the number of collisions required for an electron to be lost, but clearly it is on the order of one (not 350).

In Sec. VI we will examine possible sources of the enhanced transport of electrons in CNT that causes the confinement time to be much less than neoclassical, and also to have a component of transport proportional to $B^{-1.5}$.

VI. POSSIBLE CAUSES OF ENHANCED TRANSPORT

Experiments are currently underway using a retractable electron emitter²⁴ that creates the electron plasma as it quickly (within 20 ms) leaves the surfaces, leaving an unperturbed plasma behind. Measurements of confinement time from outside the magnetic surfaces with image charge probes or limiter probes will provide a clearer picture of the unperturbed (no rods) neutral-driven electron transport and its dependencies. Presently, however, we can evaluate whether certain candidate processes may explain the level of neutral related electron transport seen in experiments.

A. Ion accumulation

The accumulation of a small percentage of positive ions in the plasma can alter and possibly destabilize the non-neutral plasma equilibrium. Presently, ions do not continuously accumulate in the plasma even over very long time scales. This steady state in the ion content is the result of a balance between ionization of neutrals by the plasma electrons, and recombination on the insulating rods. Once the rods are removed, continuous accumulation of ions may result.

The ion density has been measured in CNT (with $B = 0.02 \text{ T}$, $V_{\text{bias}} = -200 \text{ V}$ and as a function of p_n) using a large area probe to measure the ion saturation current.¹⁸ The ion density was $n_i \approx 6 \times 10^9 \text{ m}^{-3}$ at $p_n = 2 \times 10^{-8} \text{ Torr}$, for an ion fraction of $n_i/n_e \approx 0.8\%$ in steady state. This ion fraction is consistent with estimates of the ion fraction by balancing the volumetric ionization and recombination on the rod(s).¹⁸

The ion fraction increases linearly with neutral pressure as expected from this dynamic balance, and, as mentioned, at an ion fraction of roughly 1% ion driven instabilities begin to appear.²⁵

B. Electron attachment

Another possible ionization loss mechanism is through electron attachment. If electrons are able to attach to neutrals to create negative ions, the ions will be lost quickly from the confining volume, since negative ions, being much more massive than the electrons, are very weakly magnetized at these magnetic field strengths, and are pushed out by the electron space charge, rather than confined. This loss mechanism would be roughly independent of the magnetic field strength at these low B -field strengths, and is therefore a candidate for the B -field independent neutral related loss rate that is observed. For the experiments presented here, the dominant background gases are consistent with air, i.e., about 80% N_2 and about 20% O_2 . For an electron temperature of 4 eV, typical for these experiments, the dominant negative ion formation process is dissociative electron attachment of O_2 , forming an O^- ion.²⁶ For this process, we find that $\tau_{at} \approx 10$ s for $p_n = 2 \times 10^{-8}$ Torr. Given the typical confinement times in CNT on the order of 1–20 ms, this negative ion formation cannot explain the level of transport seen in CNT.

C. Collisional transport in the $r_L \ll \lambda_D$ regime

Classical or neoclassical transport driven by collisions relies on a proper estimation of the effective collision frequency in question. In neutral plasmas, one almost always finds that $r_L \gg \lambda_D$, so the magnetic field can be ignored in the collision. In pure electron plasmas including CNT, the opposite condition exists, $r_L \ll \lambda_D$.²⁷ For example, a typical CNT pure electron plasma has $\lambda_D \approx 15$ mm, while $r_L \approx 0.3$ mm. In this limit, the magnetic field and conservation of magnetic moment μ must be considered for Coulomb collisions. The process involves $E \times B$ drift of one particle in the Debye sheath of the other particle and can lead to a factor of 100 increase in the effective collision frequency.²⁷ This may be an important effect for electron-electron collision driven transport. While electron-electron collision driven transport cannot be ruled out in CNT, it is not large enough to be experimentally identified, presently. The transport we are studying here is related to neutrals and is presumably caused by electron-neutral collisions. An elastic electron-neutral collision is accurately described in CNT as one in which the electron is unmagnetized and the neutral is infinitely massive. The electron can be considered unmagnetized since the spatial scale of the collision with the neutral is on the order of 10^{-10} m, and the Larmor radius of an electron in CNT is on the order of 10^{-4} m.

D. Transport due to unconfined particle orbits

Recently a theory for the anomalous transport of single species plasmas in Penning-Malmberg traps was proposed.^{28,29} This “asymmetry-induced transport” proceeds by the scattering of trapped particles into a velocity space loss cone. Although the scaling is not yet known in detail,²⁸ the resulting loss rate is expected to scale as $B^{-1.5}$ to B^{-2} . This is consistent with what is observed here for the neutral-driven B -field dependent transport, Fig. 8. Moreover, the re-

sults here indicate that it takes only on the order of one neutral collision to lose an electron in CNT, which also suggests that there are unconfined particle orbits in CNT. These so-called prompt orbit losses are expected for mirror (ripple) trapped particles in classical stellarators such as CNT, leading to a loss cone in phase space. However, the electric field in CNT should be sufficiently strong that orbits of mirror-trapped particles are confined, since the $E \times B$ drift forces these particles to precess poloidally rapidly compared to their ∇B drift velocities and this should close their orbits. Numerical calculations of single particle trajectories are currently underway to determine if there are unconfined orbits in CNT, despite the large electric field.

VII. PROJECTED CONFINEMENT FOR ULTRAHIGH VACUUM OPERATION WITH A RETRACTABLE EMITTER

The results presented here show that there are currently two dominant transport mechanisms in CNT, one related to neutrals, the other caused by internal rods. As mentioned, the rod driven transport can be eliminated through use of the retractable emitter, which is already installed in CNT.²⁴ The neutral driven transport is proportional to neutral pressure and can therefore be reduced by improving the vacuum in CNT. Eliminating the rod-driven transport and lowering the base pressure to 2×10^{-10} Torr should lead to a confinement time exceeding 1 s, if there are no other significant transport processes. A base pressure of 2×10^{-10} Torr has been achieved in the empty CNT chamber but has yet to be achieved with internal coils and emitter rods. Of course, other transport processes, e.g., electron-electron collisional transport, could limit the confinement in CNT and prevent the projected 1 s confinement time from being realized. Minimizing the present transport mechanisms, however, will allow the study of these other, more intrinsic, plasma transport processes in CNT.

VIII. CONCLUSIONS

Detailed studies of confinement of pure electron plasmas in the CNT stellarator were performed. The insulated rods that hold the electron emitters drive radial transport. Neutrals also drive radial transport. The rod-driven and neutral-driven transport can be separated by varying the neutral pressure. A simple model of the rod-driven transport based on negatively charged rods creating $E \times B$ convective cells was developed, and this model is in good quantitative agreement and excellent qualitative agreement with measurements of the rod-driven transport. The neutral-driven transport scales linearly with neutral pressure, except for neutral pressures above 1.5×10^{-7} Torr. It has a component that appears to be roughly independent of B , and a component that scales as $B^{-1.5}$. The transport component that is independent of the B -field is not understood at this point. The $B^{-1.5}$ scaling is not understood in detail either, but is in agreement with empirical findings from other non-neutral plasma experiments. The neutral related confinement time is on the order of the electron-neutral collision time and is orders of magnitude less than the predicted neoclassical confinement time. This

may indicate that there is a class of unconfined electron orbits in CNT, despite the large radial electric field.

ACKNOWLEDGMENTS

This work is supported by the Fusion Energy Sciences Postdoctoral Research Program of the U.S. Department of Energy, and by the NSF-DOE Partnership in Basic Plasma Science, Grant No. NSF-PHY-03-17359, and the NSF CA-REER program, Grant No. NSF-PHY-04-49813.

- ¹H. Mynick, Phys. Plasmas **13**, 058102 (2006).
- ²H. Mynick, A. Boozer, and L. Ku, Phys. Plasmas **13**, 064505 (2006).
- ³V. Nemov, S. Kasilov, W. Kernbichler, and M. Heyn, Phys. Plasmas **6**, 4622 (1999).
- ⁴A. Reiman, Plasma Phys. Controlled Fusion **41**, B271 (1999).
- ⁵D. Hartmann, Fusion Sci. Technol. **49**, 43 (2006).
- ⁶T. S. Pedersen, *New Developments in Nuclear Fusion Research* (Nova Science, New York, 2006), Chap. 5, pp. 109–123.
- ⁷T. S. Pedersen and A. Boozer, Phys. Rev. Lett. **88**, 205002 (2002).
- ⁸T. S. Pedersen, J. Kremer, R. Lefrancois, Q. Marksteiner, N. Pomphrey, W. Reiersen, F. Dahlgreen, and X. Sarasola, Fusion Sci. Technol. **50**, 372 (2006).
- ⁹R. Gandy, M. Henderson, J. Hanson, G. Hartwell, and D. Swanson, Rev. Sci. Instrum. **58**, 509 (1987).
- ¹⁰G. Lesnyakov and E. Volkov, Plasma Devices Oper. **14**, 111 (2006).
- ¹¹A. Dikii, V. Zalkind, G. Lesnyakov, O. Pavlichenko, A. Pashchenko, V. Pashnev, D. Pogozhev, and V. Tonkopyrad, Sov. J. Plasma Phys. **14**, 160 (1988).
- ¹²E. Nakamura, S. Kitajima, M. Takayama, S. Inagaki, T. Yoshida, and H. Watanabe, Jpn. J. Appl. Phys., Part 1 **36**, 889 (1997).
- ¹³H. Lin, R. Gandy, S. Knowlton, G. Hartwell, D. Prichard, G. Sassar, and E. Thomas, Phys. Plasmas **2**, 2026 (1995).
- ¹⁴J. Kremer, T. S. Pedersen, Q. Marksteiner, and R. Lefrancois, Phys. Rev. Lett. **97**, 095003 (2006).
- ¹⁵C. Hidalgo, M. Pedrosa, N. Dreval, K. McCarthy, L. Eliseev, M. Ochando, T. Estrada, I. Pastor, E. Ascasibar, E. Calderon *et al.*, Plasma Phys. Controlled Fusion **46**, 287 (2004).
- ¹⁶C. Silva, B. Goncalves, M. Pedrosa, C. Hidalgo, K. McCarthy, E. Calderon, J. Herranz, I. Pastor, and O. Orozco, Czech. J. Phys. **55**, 1589 (2005).
- ¹⁷S. Kitajima, H. Takahashi, Y. Tanaka, H. Utoh, M. Sasao, M. Takayama, K. Nishimura, S. Inagaki, and M. Yokoyama, Nucl. Fusion **26**, 200 (2006).
- ¹⁸J. Kremer, Ph.D. thesis, Columbia University (2006).
- ¹⁹J. Kremer, T. S. Pedersen, Q. Marksteiner, and R. Lefrancois, Rev. Sci. Instrum. **78**, 013503 (2006).
- ²⁰H. Saitoh, Z. Yoshida, C. Nakashima, H. Himura, J. Morikawa, and M. Fukao, Phys. Rev. Lett. **92**, 255005 (2004).
- ²¹H. Saitoh, Z. Yoshida, and S. Watanabe, Phys. Plasmas **12**, 092102 (2005).
- ²²H. Maassberg, C. Beidler, and E. Simmet, Plasma Phys. Controlled Fusion **41**, 1135 (1999).
- ²³Y. Itikawa, J. Phys. Chem. Ref. Data **35**, 31 (2006).
- ²⁴J. Berkery, T. S. Pedersen, and L. Sampedro, Rev. Sci. Instrum. **78**, 013504 (2007).
- ²⁵J. Berkery, T. Pedersen, J. Kremer, R. Lefrancois, Q. Marksteiner, A. Boozer, H. Mynick, N. Pomphrey, W. Reiersen, F. Dahlgreen *et al.*, in *Non-Neutral Plasmas VI: Workshop on Non-Neutral Plasmas, Aarhus, Denmark, 2006*, edited by M. Drewsen, U. Uggerhoj, and H. Knudsen (AIP Conference Proceedings, Melville, New York, 2006), Vol. 862, p. 62.
- ²⁶D. Rapp and P. Englander-Golden, J. Chem. Phys. **43**, 1480 (1965).
- ²⁷D. Dubin and T. O'Neil, Phys. Plasmas **5**, 1305 (1998).
- ²⁸A. Kabantsev, J. Yu, R. Lynch, and C. Driscoll, Phys. Plasmas **10**, 1628 (2003).
- ²⁹A. Kabantsev and C. Driscoll, Phys. Rev. Lett. **89**, 245001 (2002).